JOURNAL OF MATERIALS SCIENCE 29 (1994) 1075–1082

Thermal treatment effects in SiC/Al metal matrix composites

S. J. SWINDLEHURST*, I. W. HALL
Materials Science Program, University of Delaware, Newark, DE 19716, USA

A short-fibre-reinforced SiC/Al–7% Si–0.6% Mg composite has been subjected to thermal cycling and elevated temperature isothermal exposure treatments. The microstructure and residual mechanical properties have been determined as a function of these treatments. It was found that isothermal or cycling treatment at 350 °C caused severe room-temperature strength degradation while treatment at 525 °C caused little change. Strength changes are attributed principally to precipitation and dissolution effects and to transfer of magnesium from the matrix into the fibre/matrix interfacial reaction layer. There was no evidence of mechanical damage resulting from the cycling treatments.

1. Introduction

A major goal for metal matrix composite (MMC) applications is in moderate or elevated temperature environments, where they offer clear advantages over polymeric composites. Although MMCs will always have speciality applications in aerospace, larger commercial use has been anticipated to come from an exploitation of their secondary properties. A particular area of interest is in engine applications for the automotive industry where, in addition to strength, requirements include good wear and tribological properties at moderately elevated temperatures. For these applications it is important that MMCs be able to withstand prolonged thermal exposures or repeated thermal excursions while maintaining acceptable properties. MMCs become more competitive whenever demands for high specific strength and stiffness can be relaxed because lower cost reinforcements and processing techniques may be employed. Discontinuous reinforcement has an advantage in automotive applications because it allows the use of conventional and less costly methods of fabrication, such as casting, injection moulding, and powder metallurgy. Although the increases in strength and stiffness are not as great as with continuous reinforcement, significant improvements in wear resistance and temperature capability can be attained.

Much recent research has focused on SiC particulate-, whisker-, and filament-reinforced aluminium composites, particularly on the occurrence of chemical interactions between the constituents during the processing and/or subsequent steps. However, the Nicalon fibres used in the study reported below present a complex case because they contain not only SiC but also approximately 28 wt % SiO_2 and 10 wt % free carbon [1, 2]. Several studies have addressed the reactivity of SiC in the presence of aluminium, particularly with reference to the formation of carbides and, in some cases, oxides [1–7] and a brief review is presented here.

Dissolution of SiC by molten aluminium is thermodynamically feasible at temperatures above $\approx$ 600 °C [1] through the reaction

$$3SiC + 4Al \rightarrow Al_4C_3 + 3Si \quad (1)$$

Calculations [3, 6] and consideration of sections through the ternary Al–C–Si diagram [1] show that 7% Si should suppress the formation of carbide. However, when aluminium is in contact with Nicalon fibres, it can also react with the free carbon to form carbide and with the SiO_2 to form silicon and Al_2O_3 by the reaction [8–10]

$$4Al + 3SiO_2 \rightarrow 2Al_2O_3 + 3Si \quad (2)$$

This system was extensively studied by Fortier who showed that, at 727 °C, a Nicalon/pure aluminium composite should show four phases in equilibrium, namely, Al_2O_3, SiC, Al_4C_3 and an Al–4.8 at % Si liquid [2]. In contrast, a Nicalon/Al–14 at % Si composite should consist of only three phases Al_2O_3, SiC, and an Al–6 at % liquid phase. Experiments showed, however, that equilibrium was only approached slowly in the alloy matrix and that Al_4C_3 was still present even after long contact times at 727 °C. As a consequence of the sluggish disappearance of Al_4C_3 by the reverse of Reaction 2, the reaction layer was non-protective.

The presence of magnesium in the alloy used in this work may also influence the reactions, but its effect on reaction with SiC has not been thoroughly investigated. A little more is known concerning its effect on the reaction with SiO_2, a major component of Nicalon fibres. The SiO_2 surface layer on SiC and Al_2O_3 reinforcements, occurring naturally or following deliberate oxidation, has also been shown to be reduced by Al–Mg alloys during MMC fabrication to form either

* *Present address:* Laboratoire de Materiaux, Ecole Centrale Paris, 92295 Chatenay-Malabry, France.

0022–2461

spinel and/or MgO, again depending on the magnesium concentration [5, 7, 11–14]. Spinel and/or MgO are also the commonly reported reaction products in Al_2O_3/Al–Mg composites having up to 4% Mg [15–22]. For both systems this reduction reaction results in improved wetting between the alloy and reinforcement. The segregation of magnesium to the fibre–matrix interface during fabrication and/or subsequent heat treatments was cited as the cause for a decrease in age-hardening response in several MMC systems with respect to their unreinforced counterparts [11–14, 17]. The reduction reaction between SiO_2 fibres and an aluminium matrix was reported to proceed by the inward growth of Al_2O_3 towards the fibre center and an outwards diffusion of silicon during 500–600 °C heat treatments [23], resulting in a severe degradation of mechanical properties.

Therefore, the present study was undertaken to study, first, the development of the fibre–matrix interfacial region and, second, the mechanical properties as a function of the type of thermal excursions encountered in automotive applications. Adverse effects of thermal cycling, for example, would have serious consequences for many potential engine applications.

2. Experimental procedure

The composite system studied here was based on a heat-treatable aluminium alloy designated AS7G06 (Al–7% Si–0.6% Mg), reinforced with short Nicalon β-SiC fibres. This is a commonly used aluminium casting alloy with high strength, excellent castability, good corrosion resistance and weldability [24–26]. It is also a frequent choice for composite systems, because the high silicon content not only gives high fluidity for casting, but also aids in inhibiting carbide formation, while the magnesium acts as a wetting agent [4, 7, 27]. Age hardening occurs by the formation of the intermediate β′-Mg_2Si phase [25]. The Nicalon fibres, melt spun from a polycarbosilane precursor, vary in diameter from 10–20 μm. Oxygen, retained in the final fibre as SiO_2, is distributed throughout the fibre, not just in the ~ 0.1 μm thick SiO_2 surface film [1].

The SiC/Al composites were manufactured by a modified compocasting technique, using an impeller-induced vortex [28]. The fibres were preheated to remove volatile impurities and added to the semi-solid alloy at ~ 600 °C. Following full fibre incorporation, the slurry was top poured into a preheated mould and solidified under pressure to ensure intimate fibre–matrix contact and eliminate porosity. Castings were made with fibre volume fractions of 2%, 10% and 18% V_f. Unreinforced material was also produced under the same conditions. Fibre volume fraction analysis was performed on a Quantimet 970 Image Analyser using the average of 35 randomly chosen fields. TEM was performed at 100 or 120 kV on a Philips 400 (S)TEM, or on a Jeol 2000 HREM, and fractography was carried out on a Philips SEM 501 with a windowless EDS detector. Flat rectangular tensile specimens 80.3 mm × 11.6 mm × 2.6 mm were prepared in accordance with ASTM standard D3552 [29]. Tensile tests were conducted at room temperature on an 1152 Instron machine at a strain rate of 5×10^{-4} s^{-1} and at least two samples were tested in each condition.

Isothermal exposures were conducted at 350 °C for 200 h and 525 °C for 100 h, followed by furnace cooling. Some specimens were given a conventional T-6 heat treatment in order to compare the degree of metallurgical change with that in samples isothermally exposed to 525 °C.

Thermal cycling, using two fluidized sand baths, was conducted from 18 or 60 °C to 350 °C, and from 18–525 °C. The samples were unconstrained and not loaded. A maximum of 500 cycles was used with a soak duration of 4 min at each temperature (equivalent to ~ 33 h exposure to the elevated temperature). Some samples were subjected to a limited run of only 10 cycles from 18–350 °C in order to determine how rapidly the effects of thermal cycling appeared. Unfortunately, during thermal cycling of the unreinforced samples to 525 °C severe warpage occurred and no mechanical property data were obtained.

Although temperature excursions in typical applications would not exceed about 350 °C, the more rigorous regimes employed here were used as a way both of accelerating any damage process and of studying possible metallurgical effects at elevated as well as intermediate temperatures.

3. Results

3.1. Mechanical properties

The tensile data for the as-cast material are presented in Fig. 1a as a function of volume fraction of reinforcement. (The error bars in this figure illustrate a spread of data which was typical for all the tests in this research.) All the mechanical properties increased slightly then dropped precipitously before recovering somewhat. All samples failed at relatively low strains.

Simple isothermal exposure at 350 °C, Fig. 1b, produced drastic reductions in the tensile properties of both the unreinforced matrix and the composites when compared with as-cast material. The failure strain of specimens containing 2% V_f reinforcement, however, increased to an astonishing 16%, more than four times the value for the unreinforced alloy. Perhaps more surprising, was that isothermal exposure at a still higher temperature, 525 °C, yielded properties which were only slightly different from the as-cast values for all the materials, Fig. 1c.

Cycling from 60–350 °C caused no changes in strength for the unreinforced alloy but caused a marked decrease in strength in the composites, Table I. Cycling from 18–350 °C, on the other hand, produced a marked drop in the mechanical properties of the matrix as well. The data for 18% V_f samples show that the decrease in mechanical properties begins very early in the testing procedure and that ~ 50% of the strength reduction noted after 500 cycles had already occurred after 10 cycles. In all instances, the loss in strength tended towards the values induced by isothermal exposure to the same temperature.

Finally, thermal cycling from 18–525 °C resulted in a dramatic increase in yield strength from 60 MPa to

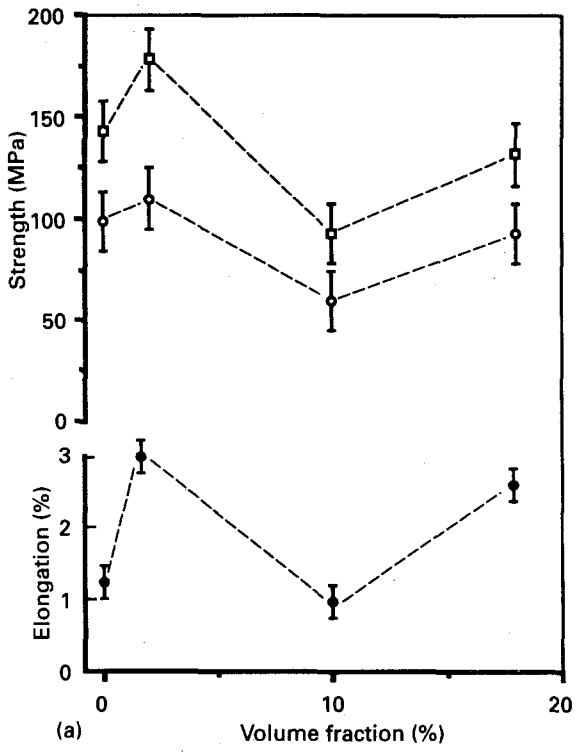

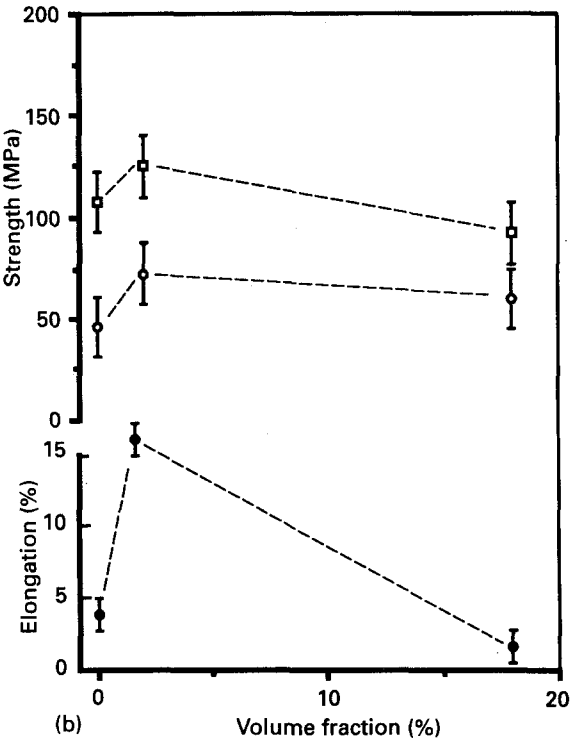

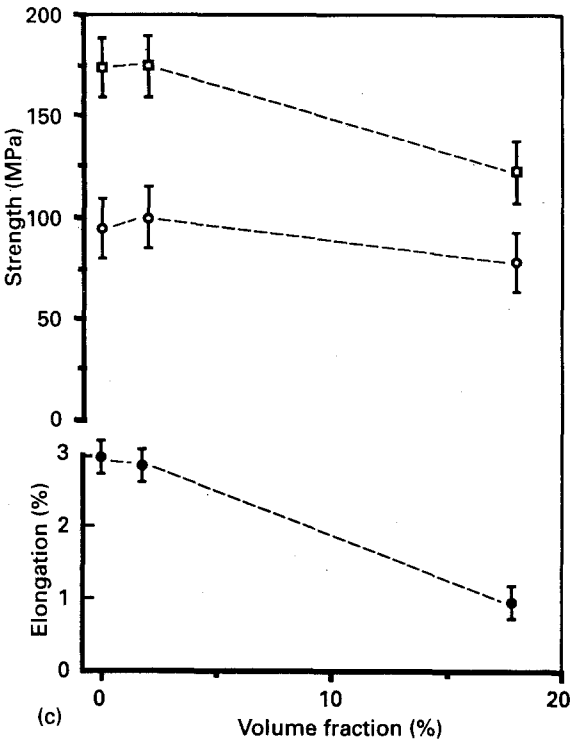

Figure 1 Tensile data: (a) as-cast, (b) after isothermal exposure for 200 h at 350 °C, and (c) after isothermal exposure for 100 h at 525 °C. (□) Ultimate strength, (○) yield strength, (●) elongation.

TABLE I Mechanical properties of thermally cycled samples

Sample (% V_f)	Thermal cycling treatment	Yield strength (MPa)	Ultimate strength (MPa)	Failure strain (%)
0	None	99	143	1.2
2	None	110	178	3.0
10	None	60	93	1.0
18	None	93	132	2.6
2	500 cycles 60–350 °C	99	154	1.1
10	500 cycles 60–350 °C	39	73	1.8
18	500 cycles 60–350 °C	78	131	0.9
0	500 cycles 18–350 °C	58	121	3.6
18	10 cycles 18–350 °C	85	140	0.6
18	500 cycles 18–350 °C	76	125	0.9
10	500 cycles 18–525 °C	112	180	1.2
18	500 cycles 18–525 °C	93	125	0.5

112 MPa for the 10% V_f composites, with a corresponding increase in ultimate strength. The same treatment had no significant effect on the higher volume fraction material.

3.2. Microstructural observations

In the as-cast condition, the microstructure consisted of primary α-aluminium dendrites surrounded by an interdendritic eutectic network of angular silicon flakes and script π-$Al_8FeMg_3Si_6$ particles. The fibres were randomly oriented and located primarily in the interdendritic regions, Fig. 2a. The fibre distribution was moderately homogeneous for 2% and 10% V_f samples, but 18% V_f samples showed occasional regions where the fibres had agglommerated. Also, in contrast with lower % V_f, the ragged, uneven borders of the fibres in 18% V_f indicated that they had reacted with the matrix, Fig. 2b. This, together with the presence of more extensive shrinkage cavities than were found in lower % V_f samples, led to the conclusion that the intended processing temperature was exceeded for 18% V_f, probably as a result of the difficulty of mixing in the larger V_f of fibres.

TEM and EDS showed numerous precipitates of varying morphologies and compositions in the interdendritic regions. Mg_2Si and various Al/Si/Fe/Mg

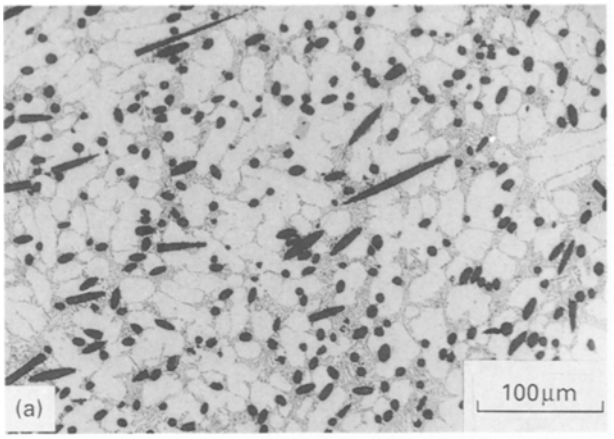

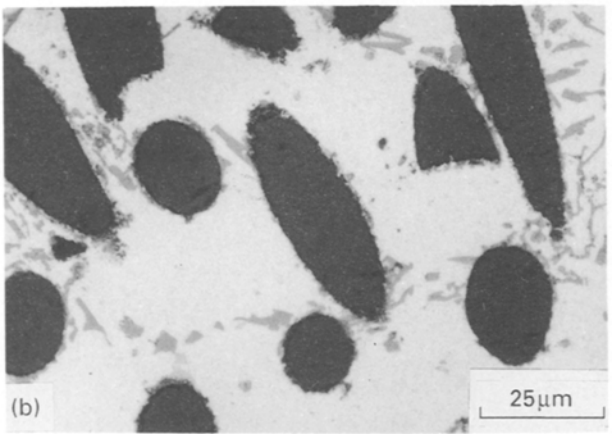

Figure 2 (a) As-cast 18% V_f material and, (b) higher magnification showing evidence of fibre/matrix reaction.

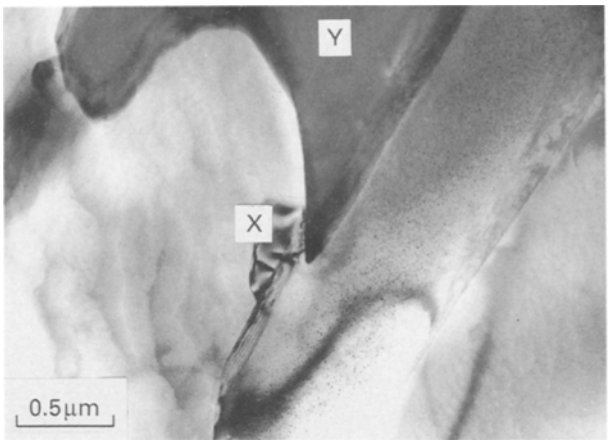

Figure 3 Transmission electron micrograph showing the morphology of silicon and second-phases particles, Mg_2Si, π-$Al_8FeMg_3Si_6$ (marked X and Y, respectively).

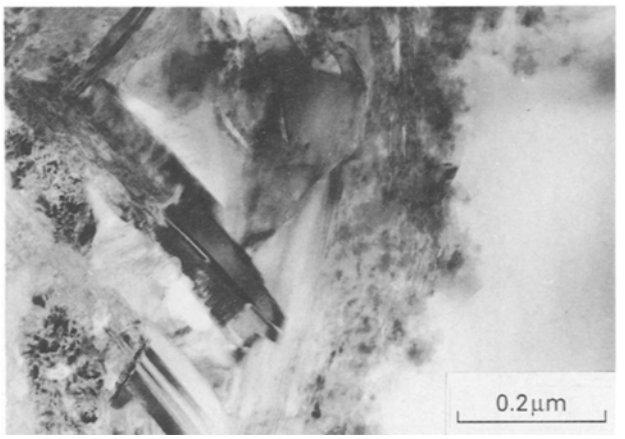

Figure 4 Interphase of 18% V_f sample showing silicon and Al_4C_3 plate-like crystals.

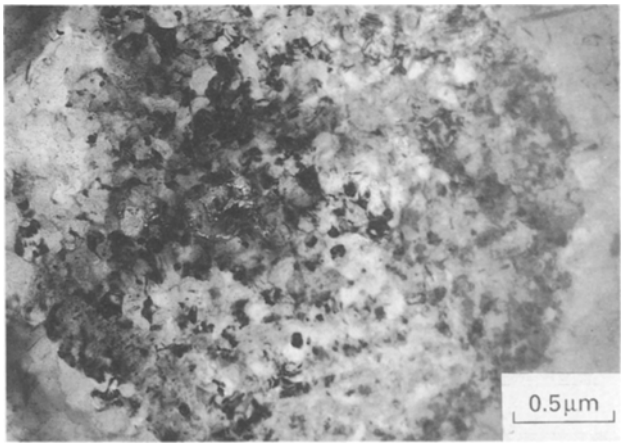

Figure 5 A fibre, ~ 3 μm diameter, completely consumed by reaction.

compounds were frequently located in close association with the eutectic silicon flakes, Fig. 3. The fibre–matrix interfacial region was a continuous layer approximately 400 nm thick for 2% and 10% V_f samples and 650 nm for 18% V_f samples, consisting of a complex zone of a microcrystalline interphase, small silicon crystals, discrete needles of Al_4C_3, and other precipitates, Fig. 4. Spotty ring electron diffraction patterns showed the interphase to consist primarily of γ-Al_2O_3 and identification of the Al_4C_3 needles was confirmed by lattice imaging. Wet chemical analysis of 18% V_f samples confirmed that they contained 0.7% volume fraction of Al_4C_3.

A few partially or completely reacted fibres were also found, Fig. 5. These fibres were always well below the average size, being initially only 2–4.5 μm diameter. Small crystals could be resolved within this interaction zone, particularly towards the zone–matrix boundary. This zone was examined by (S)TEM in conjunction with EDS; only the elements of aluminium, silicon, and magnesium were found, in various combinations.

Isothermal exposure or cycling to 350 °C produced no differences in optical microstructures from the as-cast condition, apart from slight rounding of the eutectic silicon crystals in the composites following simple exposure. However, TEM showed significant coarsening of the precipitates in the interdendritic regions with respect to their as-cast condition, particularly for the isothermal exposure. Although the fibre–matrix interfacial layer remained basically unchanged in thickness and appearance, diffraction patterns taken from this region became more complex

and both γ-Al_2O_3 and $MgAl_2O_4$ were identified in the interfacial region.

Thermal exposure at 525 °C effectively broke up the interdendritic continuity by spheroidizing the silicon and Al/Fe/Mg/Si phases; only a slight coarsening of the precipitates resulted. However, γ-Al_2O_3. $MgAl_2O_4$, and MgO were found in the interfacial region of these specimens.

Cycling to 525 °C and the T-6 treatment also caused spheroidization, though not to as great an extent. However, a very fine distribution of precipitates was observed, Fig. 6. These secondary phases and Mg_2Si crystals were much smaller than those even in the as-cast structure. No evidence of mechanical damage to the fibres or of void formation at the fibre–matrix interface was ever observed. The interfacial region consisted of γ-Al_2O_3 and MgO, as was also the case for T-6 treated samples. Moreover, elemental concentration profiles for magnesium, silicon and aluminium taken at the fibre–matrix interface confirmed a definite enrichment of magnesium in the interfacial zone.

3.3. Fractography

The ductility exhibited by all of the as-cast samples was low and the failure mode was mixed, consisting predominantly of cleavage facets of fractured silicon flakes separated by regions of ductile dimples arising from the aluminium matrix. Fibre/matrix bonding was very strong. Negligible pull-out was observed in fibres oriented parallel to the tensile axis, and those oriented transversely remained so firmly adhered to the matrix that they failed by cleaving along their lengths, Fig. 7. A thin layer of reaction product could occasionally be seen along the edges of cleaved fibres and, particularly in 18% V_f samples, more heavily reacted fibres were also sometimes found, Fig. 8.

Thermal exposure at 350 °C caused marked matrix softening in all cases, as noted above, but the ductility of the unreinforced material was still limited by brittle failure of the angular silicon flakes. In the MMC samples, the slight spheroidization of the silicon phase was apparently sufficient to modify the failure mode and the fracture surfaces were strikingly different from their as-cast counterparts: failure occurred cumulatively in the matrix through extensive plastic deformation, resulting in a fracture surface composed of microdimples throughout the matrix and cleaved fibres. It is of interest to note that, even at the high strains experienced by 2% V_f samples, the fibre–matrix bond remained intact, as attested by the presence of matrix ligaments still adhering to the fibre surface, Fig. 9. Moreover, the fibres did not serve as crack initiators and they underwent multiple fragmentation as the matrix continued to flow about them.

Thermal exposure at 525 °C caused marked spheroidization of the silicon crystals, raising the ductility of the matrix somewhat. This was reflected in the fracture surfaces of all samples, which showed a "honeycomb" structure of relatively large, equiaxed dimples nucleated on fibres and rounded silicon grains, Fig. 10. Again, the fibres remained very well bonded to the matrix.

For specimens thermally cycled to 350 °C, there was little discernible difference between their fracture surfaces and those of their as-cast counterparts; all exhibited mixed cleavage and ductile failure modes.

The fracture surfaces of 2% and 10% V_f samples cycled from 18–525 °C also consisted of a honeycomb

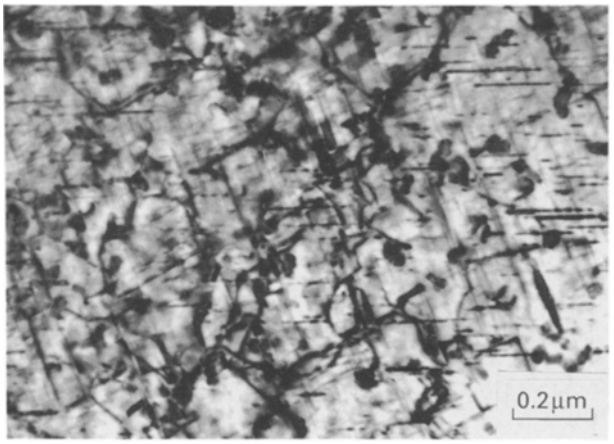

Figure 6 Fine-scale precipitation of rod-like Mg_2Si after cycling to 525 °C.

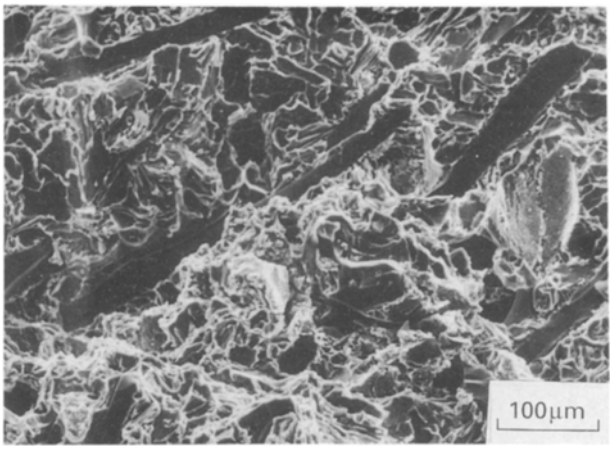

Figure 7 Fractograph of 2% V_f composite showing longitudinal fibre splitting and cleavage of silicon.

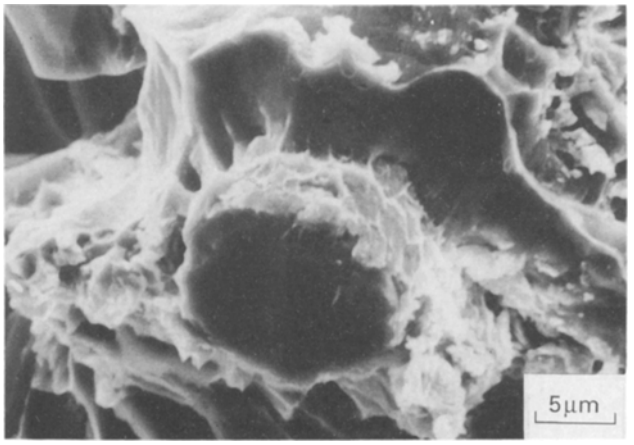

Figure 8 Fractograph of 18% V_f sample showing the surface of a reacted fibre.

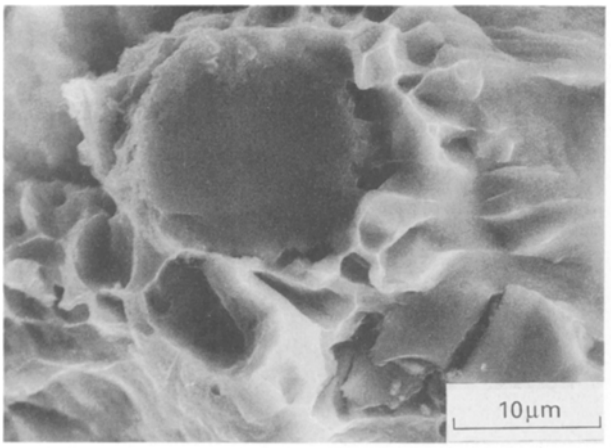

Figure 9 Fractograph of 2% V_f sample showing excellent adherence of matrix to fibre.

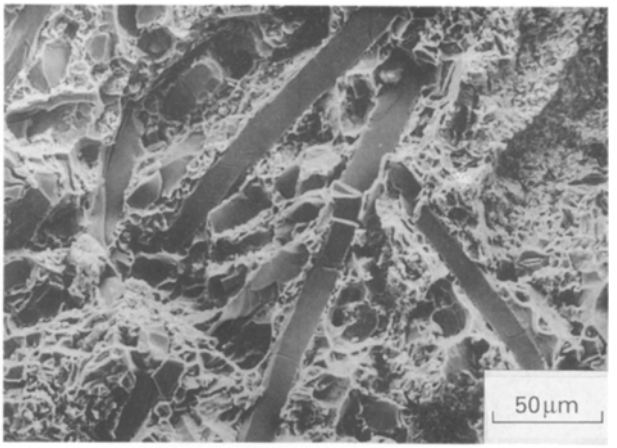

Figure 11 Fractograph of 18% V_f sample cycled from 18–525 °C showing cleaved fibres and a dimpled rupture in the matrix.

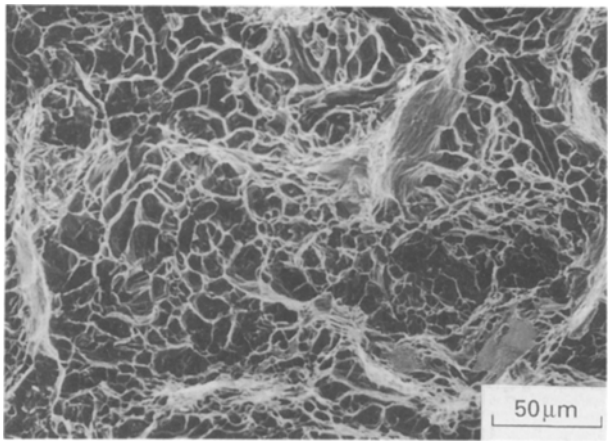

Figure 10 Fractograph of 10% V_f sample isothermally exposed at 525 °C showing coarse dimples.

structure of relatively coarse equiaxed dimples, though the dimples were smaller than those of samples exposed to 525 °C. 18% V_f specimens, on the other hand, showed very little of the honeycomb structure and resembled more the 350 °C isothermally exposed samples, with failure occurring by microdimple formation throughout the matrix, Fig. 11.

Throughout these observations, the major changes occurred in the fracture morphology of the aluminium matrix itself and none of the potential types of damage caused by thermal cycling, such as fibre cracking, fibre debonding, void formation, or dimensional change, was observed in these systems.

4. Discussion

4.1. Fibre–matrix interface

It has been shown here that the fibre–matrix interface region consists of a layer of oxides with small crystals of silicon and aluminium carbide in its outer periphery. TEM observations confirm that reactions 1 and 2 have occurred during fabrication of the composite material. However, carbide formation was not extensive in the present system and did not appear to be detrimental to the composite properties.

The thickness of the observed interfacial reaction layer and its identification as primarily Al_2O_3 clearly shows that the SiO_2 in the fibre itself is reacting, not simply the 100 nm thick surface layer. The observation that some undersized fibres had been completely consumed by the reaction further confirms that the entire fibre is reacting. Because the oxide forms by partial dissolution of the fibre and proceeds by an inward migration of aluminium, it is probable that it "keys" into the fibre, thus explaining the strength of the fibre–matrix bond. In most of the fibres, the extent of this attack was minimal, involving only a fraction of the total fibre radius.

Even though magnesium is the stronger reducing agent, the SiO_2 layer is reduced by aluminium due to its much higher concentration in the alloy. During the reduction reaction, the γ-Al_2O_3 grows inwards towards the fibre centre, and small silicon precipitates form and partially encase the fibres, limiting further reaction [22, 23]. Hence the small silicon crystals and aluminium carbides outline the original perimeters of the fibres as observed. With higher processing temperatures, greater portions of the fibres are consumed by the reaction and a more crystalline oxide zone results, as seen in the 18% V_f composites.

Observations of monolithic Al–Mg alloys have shown that over long times at temperatures above 350 °C, magnesium can diffuse through the matrix and dope the oxide zone [30]. Then, depending on the temperature regime, the magnesium eventually reduces the γ-Al_2O_3 to form either spinel or MgO. Our observations confirm that the intermediate temperatures (i.e. $\leqslant$ 350 °C) tend to favour the formation of spinel alone within the interfacial region, whereas the 525 °C treatments promote the growth of MgO, although spinel also forms on continued exposure. Diffusion of magnesium from the matrix to the interfacial region was verified by concentration profiles (EDS line scans), which revealed local magnesium depletion in the matrix and magnesium enrichment within the interfacial region. Segregation of magnesium to an

oxide interfacial region has been previously reported for other composite systems [11–14, 17].

Overall, morphological changes occurring within the reaction zone of these compocast composites correspond well with the oxidation behaviour of the monolithic alloy. Nevertheless, it is important to point out that, regardless of these reactions, the fibres remained strongly bonded to the matrix. This last point supports previous conclusions which suggested that spinels or similar oxides may be used to promote interfacial bonding, due to their potential to form strong bonds with both metals and ceramics [15].

It should also be noted that the oxide layer did not thicken as a result of the thermal treatments, indicating that the dissolution of the fibre does not continue, nor does external oxygen diffuse into the system to promote oxide growth at the matrix–interfacial region boundary. This is fortunate because continued fibre degradation would probably result in a further reduction in mechanical properties.

4.2. Mechanical properties

Several features of the mechanical property data deserve particular mention, beginning with the anomalous room-temperature behaviour, whereby the MMCs exhibited reduced strength compared with the matrix. The effect is considerably larger than predicted by simple calculations of the critical volume fraction for reinforcement and has been reported in other short-fibre-reinforced aluminium systems as well [31–33]. For example, the introduction of $\sim 24\%$ Saffil δ-Al_2O_3 fibres to an Al–7 Si matrix was shown to result in a 25%–30% decrease in strength compared with the unreinforced alloy, and $> 50\%$ V_f was necessary for any net strengthening to occur [31]. A rule of mixtures model, modified to account for the finite fibre lengths and the non-axial fibre distribution, was developed by Friend to explain this phenomenon [31]. It was shown that for some systems, a region could exist over which there was a decrease in strength with increasing fibre volume fractions, attributable to the low reinforcement efficiency in pseudo-three-dimensional fibre arrays.

The second notable observation was the pronounced decrease in strength occurring with cycling or exposure treatments up to 350 °C. Surprisingly, the corresponding strength reductions were usually considerably less after treatments at 525 °C and thermal cycling from 18–525 °C even resulted in a dramatic increase in strength for the 10% V_f composites. Because there was not the slightest evidence of damage occurring as a result of thermal cycling, it must be concluded that this behaviour arose from simple metallurgical precipitation effects resulting from the cycling or heat-treatment schedules. Thermal treatments at intermediate temperatures are sufficient to cause recovery, precipitate coarsening and other softening processes but insufficient to cause complete precipitate dissolution and re-precipitation phenomena. This was confirmed in the present work by TEM which showed that, after treatments at 350 °C, the precipitates were significantly overaged. Magnesium depletion from the matrix grains, thereby suppressing the formation of Mg_2Si, may also play a significant role.

Matrix softening was minimal in specimens isothermally exposed to 525 °C, and only a slight coarsening of the precipitates was observed. It is believed that the precipitates redissolve at the treatment temperature and re-precipitate during cooling, much as when fabricated. The modest decrease in strength of the 18% V_f material was probably due to the greater loss of magnesium which could be expected in the higher V_f composites. Because the specimens were furnace cooled, it is also probable that the slight loss in strength reflects a decrease in the levels of thermal residual stress over those generated during fabrication.

Cycling to 525 °C, on the other hand, was followed by a relatively rapid cool and the resulting Mg_2Si precipitate distribution closely resembled that found after conventional age-hardening treatments.

A similar dramatic decrease in strength at intermediate exposure temperature was observed previously in a SiC whisker/2124-T6 aluminium composite following isothermal exposure or thermal cycling to 300 °C [34]. It was determined in that study that the loss in strength was also governed by precipitate overageing.

Finally, it is clear that thermal cycling is itself no more detrimental than isothermal exposure alone. No further damage mechanisms are found and the effect of thermal cycling is seen to be broadly the same as would be produced by simple isothermal exposure for an equivalent period of time. This is encouraging for further development of these materials in areas where thermal excursions are unavoidable.

5. Conclusions

The work presented here examined potential problems which may be encountered due to the effects of long-term exposure to elevated temperatures and of thermal cycling. The main conclusions are listed below.

1. Precipitate strengthening plays a significant role in this SiC/Al system, particularly with respect to its behaviour in a thermal environment.
2. Overageing was the primary cause for the loss in strength of SiC/Al MMCs subjected to various thermal treatments.
3. There was no evidence of mechanical damage resulting from thermal cycling.
4. The amount of silicon present in the alloy was ineffective in suppressing carbide formation.
5. The interfacial reaction layer enhances fibre–matrix bonding, without detriment to the other material properties.

Acknowledgements

The authors thank the Center for Composite Materials, University of Delaware, and the Laboratoire de Chimie du Solide du CNRS, University of Bordeaux I, Bordeaux, for material supply and partial financial support during the course of this research.

References

1. C. H. ANDERSSON, PhD dissertation, Chalmers University of Technology, Sweden (1983).
2. P. FORTIER, PhD dissertation, Université Claude Bernard-Lyon I, France (1988).
3. G. SELVADURAY, R. HICKMAN, D. QUINN, D. RICHARD and D. ROWLAND, in "Interfaces in Metal Ceramic Composites", edited by R. Y. Lin, R.J. Arsenault, G. P. Martins and S. G. Fishman (TMS, Philadelphia, PA, 1986) p. 271.
4. C. MILLIERE, PhD dissertation, Institut National Polytechnique de Grenoble (1986).
5. J. G. LEGOUX, L. SALVO, H. RIBES, G. L. L'ESPÉRANCE and M. SUÉRY, in "Interfaces in Metal-Ceramic Composites", edited by R. Y. Lin, R.J. Arsenault, G. P. Martins and S. G. Fishman (TMS, Philadelphia, PA, 1986) p. 187.
6. D. LLOYD, *Compos. Sci. Technol.* **35** (1989) 159.
7. A. BARDAL and R. HØIER, in "Metal Matrix Composites—Processing, Microstructure and Properties", Proceedings of the 12th Risø International Symposium on Material Science, edited by N. Hansen, D. Juul Jensen, T. Leffers, H. Lilholt, T. Lorentzen, A. S. Pedersen, O. B. Pedersen and B. Ralph (Risø National Laboratory, Roskilde, 1991) p. 205.
8. A. STANDAGE and M. S. GANI, *J. Am. Ceram. Soc.* **50** (1967) 101.
9. K. PRABRIPUTALOONG and M. R. PIGGOT, *ibid.* **56** (1973) 184.
10. *Idem, J. Electrochem. Soc. Solid State Sci. Technol.* **127** (1974) 430.
11. R. DASILVA, D. CALDEMAISON and T. BRETHEAU, in "Mechanics and Mechanisms of Damage in Composites and Multi-Media Materials", ESIS-11, edited by D. Baptiste (Mechanical Engineering Publications, London 1991) p. 395.
12. H. RIBES, M. SUÉRY, G. L'ESPÉRENCE and J. G. LEGOUX, *Metall. Trans.* **21A** (1990) 2489.
13. C. M. FRIEND, R. YOUNG and I. HORSFALL, in Proceedings of ECCM 1: Developments in Science and Technology of Composite Materials, edited by A. R. Bunsell, P. Lamicq and A. Massiah (AEMC and CODEMAC, Bordeaux, 1985) p. 227.
14. H. RIBES and M. SUÉRY, *Scripta Metall.* **23** (1989) 705.
15. C. LEVI, G. ABBASCHIAN and R. MEHRABIAN, *Metall. Trans.* **9A** (1978) 697.
16. B. F. QUIGLEY, G. J. ABBASCHIAN, R. WUNDERLIN and R. MEHRABIAN, *ibid.* **13A** (1982) 93.
17. A. D. MCLEOD and C. M. GABRYEL, *ibid.* **23A** (1992) 1279.
18. A. MUNITZ, M. METZGER and R. MEHRABIAN, *ibid.* **10A** (1979) 1496.
19. K. SUGANUMA, T. OKAMOTO, T. HAYAMI, Y. OKU and N. SUZUKI, *J. Mater. Sci.* **23** (1988) 1318.
20. C.-F. HORNG, S.-J. LIN and K.-S. LIU, *Mater. Sci. Eng.* **A150** (1992) 290.
21. B. C. PAI, *ibid.* **24** (1976) 31.
22. R. A. PAGE, J. E. HACK, R. SHERMAN and G. R. LEVERANT, *Metall. Trans.* **15A** (1984) 1403.
23. H. V. SQUIRES and H. W. RAYSON, *J. Mater. Sci.* **12** (1977) 1010.
24. S. MURALI, K. S. RAMAN and K. S. S. MURTHY, *Mater. Sci. Eng.* **A151** (1992) 1.
25. N. HAN, G. POLLARD and R. STEVENS, *Mater. Sci. Technol.* **8** (1992) 52.
26. M. VEDANI, G. PIATTI and C. DIGREGORIO, in "Mechanics and Mechanisms of Damage in Composites and Multi-Media Materials", ESIS11, edited by D. Baptiste (Mechanical Engineering Publications, London, 1991) p. 407.
27. M. GUPTA *et al.*, in "Fundamental Relations Between Microstructures and Mechanical Properties of Metal Matrix Composites", Proceedings of the Symposium TMS 1990 Fall Meeting, edited by P. K. Liaw and M. N. Gungor (TMS, Warrendale, PA, 1990) p. 3.
28. F. GIROT, PhD dissertation, Université de Bordeaux I, France (1987).
29. "Standard Test Methods for Tensile Properties of Metal Matrix Composites", Vol. 10. Annual Book of ASTM Standards (ASTM, Philadelphia, PA, 1982).
30. J. M. RITCHIE, J. V. SANDERS and P. L. WELCKHARDT, *Oxid. Metals* **3** (1971) 91.
31. C. M. FRIEND, *J. Mater. Sci.* **22** (1987) 3005.
32. M. MANOHARAN and J. J. LEWANDOWSKI, *Mater. Sci. Eng.* **A150** (1992) 183.
33. F. J. HUMPHREYS, in "Mechanical and Physical Behavior of Metallic and Ceramic Composites", edited by S. I. Anderson, A. Lilholt and O. B. Pedersen (Risø National Laboratory, Roskilde, 1988) p. 51.
34. I. W. HALL and W. G. PATTERSON, *Scripta Metall. Mater.* **24** (1991) 805.

Received 15 April
and accepted 20 August 1993